

Modelling the solar photospheric plasma and magnetic field dynamics during the emergence of AR 11190

Campos Rozo, Jose Ivan^{1,2}; Utz, Dominik^{1,3}; Veronig, Astrid¹;
Vargas Dominguez, Santiago²

¹ Institute of Physics/IGAM, University of Graz, Graz, Austria

² Observatorio Astronómico Nacional, Universidad Nacional de Colombia, Bogotá, Colombia.

³ Instituto de Astrofísica de Andalucía IAA-CSIC, Granada, España.

Abstract

The interaction between the plasma and the magnetic field has been studied before by various authors. In this work we will show a detailed study employing two different distributions applied to the flow velocities during the emergence and prior evolution of AR 11190 on 11-April-2011. The velocity fields are computed from intensity as well as LOS magnetograms by using Local Correlation Tracking (LCT) techniques. Horizontal velocities as well as vertical velocities show strong correlation between the emergences of new fast and strong positive magnetic elements, and strong divergences observed from vertical velocities calculated by LCT in continuum data. Although there are several divergence regions within the field of view, just the region of interest shows the emergences of new magnetic field.

1. INTRODUCTION

The solar photosphere shows on its surface different features related with the emergence of convective flows, transporting plasma, energy as well as magnetic field from the solar interior. The plasma emergences display flow convective patterns called granulation, mesogranulation, and supergranulation, depending on the spatial and temporal dimension of their organization and evolution. On the photosphere it is also possible to observe the arrangement of magnetic field at different scales, from small-scales, like Magnetic Bright Points (MBP; Utz, D. et al. 2010), to large-scale magnetic concentrations such as Sunspots (Solanki, S. K., 2003) or Active Regions (AR). Different Local Correlation Tracking (LCT) techniques have been used for the analysis of these features. LCT was applied for the first time by November and Simon (1988). The algorithm is based on the idea to find the best cross-correlation between the intensities of two consecutive images in t , and $t+\tau$, time instances. Besides, the plasma vertical intrinsic emergences, the photospheric evolution is strongly influenced by the expansion and fragmentation of the granules. The meso- and supergranules have been associated to fast emergence flows (Palacios et al. 2012), as well as to explosive granules, which occur

with higher frequencies in mesogranule regions (e.g. Title et al. 1989), or during the emergence of magnetic field, and its subsequent accumulation in intergranular zones (Domínguez Cerdeña 2003; Ishikawa & Tsuneta 2011).

2. DATA

On April, 11, 2011 an active region started to form on the solar disk. We focused in this AR 11190 (see Fig. 1). Here it was possible to observe the time instances of the emergence and formation of the AR. The used data covers the 24 hours of April 11, 2011 during the first formation stage of the AR, and consists of continuum image data, as well as Line Of Sight - LOS magnetograms, taken with the Helioseismic and Magnetic Imager (HMI; Hoeksema et al. 2014) on board of the Solar Dynamics Observatory (SDO; Pesnell et al. 2012) spacecraft. The cadence for intensity maps as well as for magnetic field images is 45 seconds, whereas the pixel size corresponds to ~ 0.504 arcsec/pix.

The data need to be prepared before the analysis can be started (e.g. de-rotation, co-alignment, subsonic-filtering). All the preparation and analysis have been done using Python programming language, and the specialized library for the solar data analysis SunPy

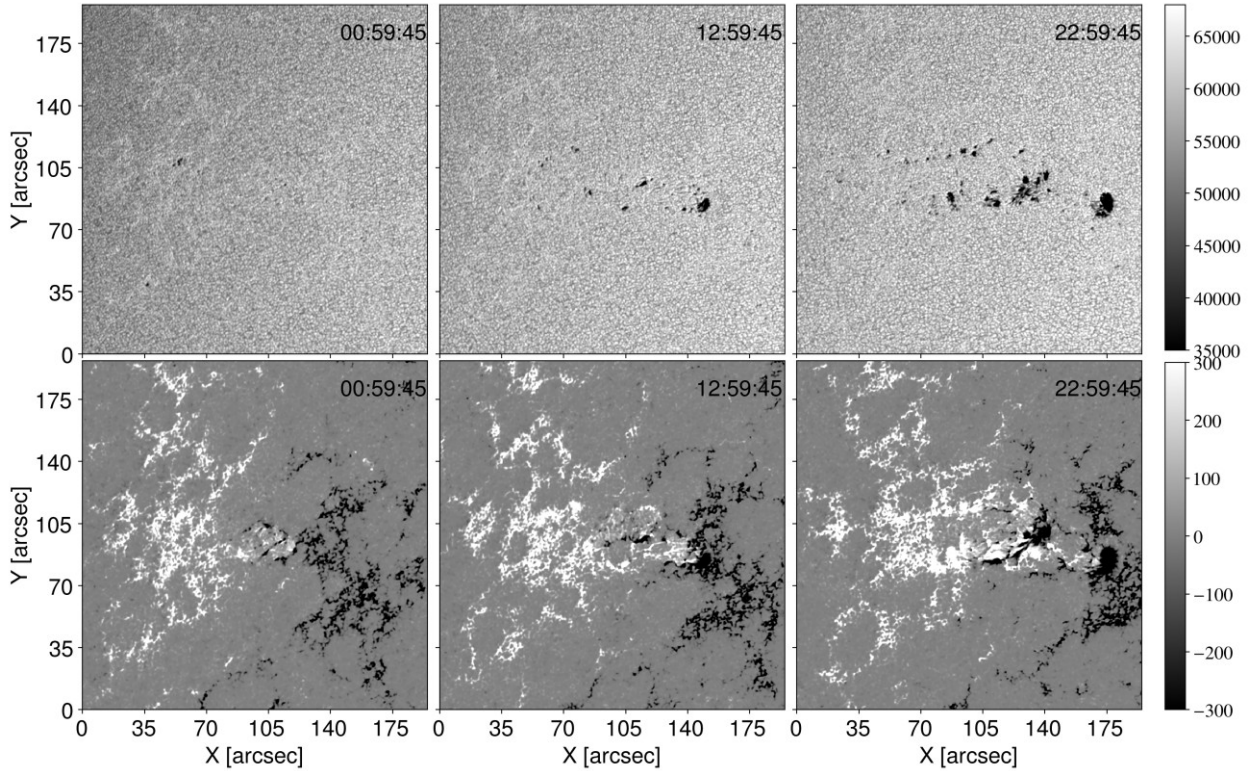


Figure 1. Temporal evolution during the emergence of AR 11190 on April 11, 2011. [Top] Continuum images enhanced for double resolution (~ 0.25 arcsec/pix). [Bottom] LOS magnetograms with the same resolution after application of the enhancing algorithm.

(SunPy Community et al. 2015). As the calculations of proper motions are dependent on the resolution of the data, we improved the resolution of the HMI data (continuum images as well as the LOS magnetograms) using the new enhancing algorithm, described in Diaz Baso, C. J. et al (2018).

3. ANALYSIS AND RESULTS

We focused on the tracking and dynamic behaviour of the horizontal and vertical velocity fields obtained from intensity as well as magnetic field maps during the formation instances of AR 11190. Emergence flows are associated to meso- and supergranules (Palacios et al. 2012). Thus, to be able to detect these flows, we have chosen the size of the correlation window FWHM as 12.5 arcsec that are correlated with average size for mesogranules (~ 9 Mm; November et al., 1981), and applied a temporal average of 2 hours (Life-time average for mesogranules; ver Hill et al.1984; Rast 2003). The LCT algorithm used in the present work is given by

$$C_{t,t+\tau}(\delta, \mathbf{x}) = \int J_t(\zeta - \delta/2) J_{t+\tau}(\zeta - \delta/2) W(\mathbf{x} - \zeta) d\zeta, \quad Eq. 1$$

where $C_{t,t+\tau}(\delta, \mathbf{x})$ represents the coordinates of the position as well as the displacements in both directions, x , and y . The terms J_t , and $J_{t+\tau}$ represent the intensity values for two consecutive images. Times t , and $t+\tau$ are

the time instances of the two images, and the $W(\mathbf{x} - \zeta)$ function is an apodization window, that for our particular case, was chosen to be represented by a Gaussian window, defined by the value FWHM as mentioned before.

Figure 1 shows three time instances of the evolution during the formation of AR 11190. The top row displays the continuum images, whereas the bottom row shows the evolution of LOS magnetic field. Clearly one can observe the fast emergence of positive magnetic field in the center of the Field of View (FOV) that pushes the pre-existent magnetic elements away.

The first row in Fig. 2 shows the horizontal velocities calculated from the continuum data. Contour levels represent the vertical positive velocities overplotted on the maps with the background being associated with the time instances shown in each image. Second row displays the horizontal velocities obtained from LOS magnetograms plotted over the maps at the respective times, where the red arrows represent the horizontal velocities associated with proper motions of fast and strong positive magnetic elements (> 50 G), whereas the blue arrows are connected with strong and fast negative magnetic elements (< -50 G).

The behaviour of the horizontal flow fields displayed in Fig. 2 show how the formation of the AR 11190 is led by the fast and violent emergence of new strong positive magnetic elements in the center of the FOV, pushing the previous positive and negative magnetic

field. It is possible to observe that whereas the center of the field of view seems to emerge following radial motions, in general, the magnetic field has strong motions to the right.

Figure 3 shows vertical velocities calculated using the idea of the divergence between the horizontal velocities v_x , and v_y , leading to v_z via

$$v_z(v_x, v_y) = h_m \nabla \cdot v_h(v_x, v_y), \quad \text{Eq. 2}$$

where h_m is a constant and represents the mass flux scale (see *November et al. 1981*). The background maps represent the vertical velocities obtained from the intensity maps (plasma motions), and the white contour lines represent the positive vertical velocities with values of [0, 1, 1.5, 2, 2.5] km/s.

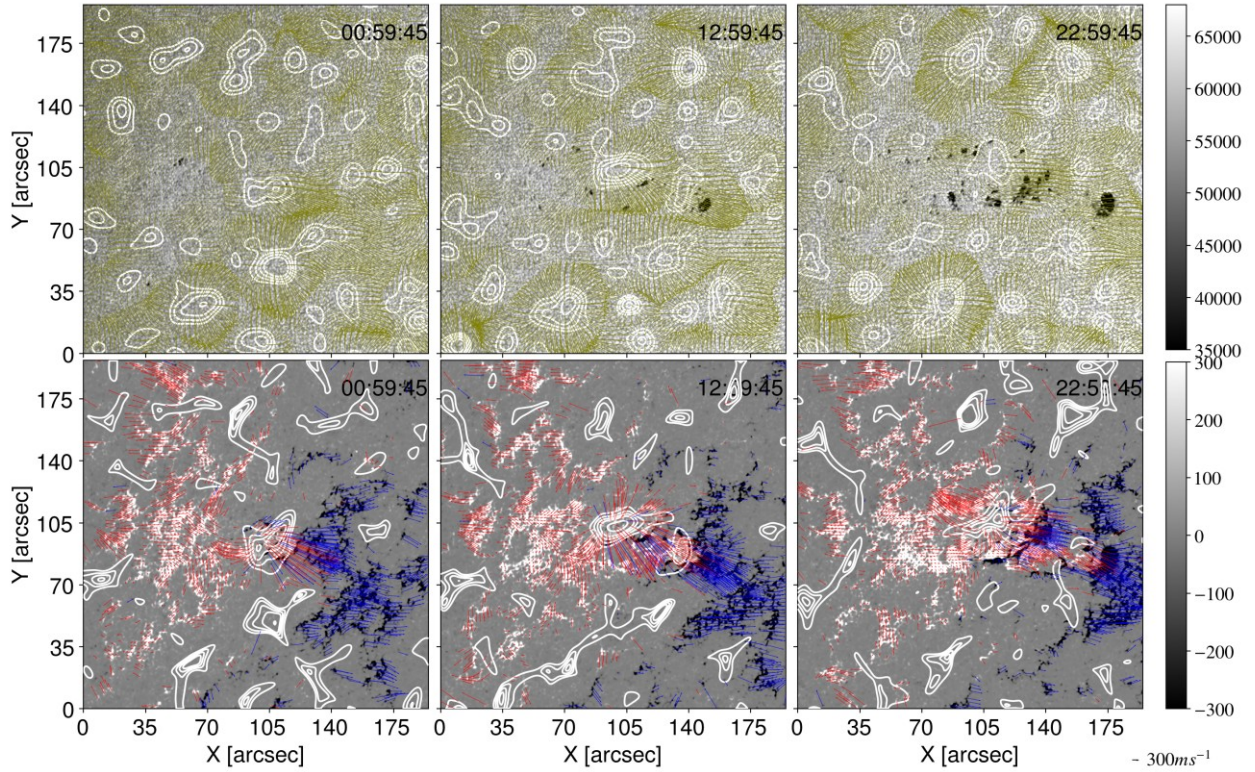


Figure 2: Temporal evolution of the horizontal velocity fields. [Top] Plasma horizontal velocities with positive vertical velocities plotted by the white contours. The contour lines represent velocity values of [0, 1, 1.5, 2, 2.5] km/s. [Bottom] Horizontal velocities calculated from the LOS magnetograms. Contour lines represents again positive vertical velocities with the values mentioned before. The arrow in the right lower corner represents a vector with a magnitude of 0.3 km/s.

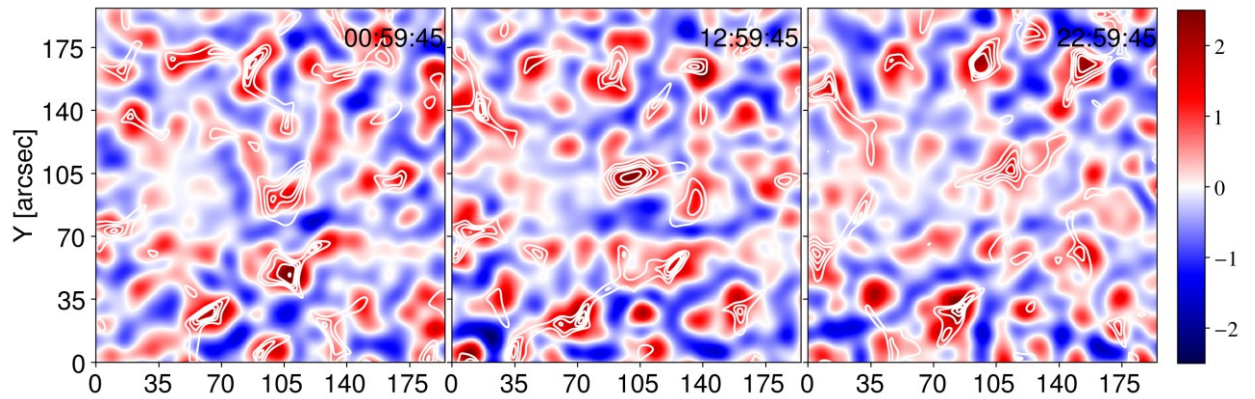


Figure 3: Temporal evolution of the vertical velocity fields. The figure shows the correlation between vertical velocities calculated from continuum maps, and vertical velocities obtained from LOS magnetograms. Background maps are vertical velocities from intensity maps, whereas contour lines represent positive vertical velocities from LOS magnetic fields. The color map represent the vertical velocities in the background in km/s.

Although the plasma flow fields shows fast divergences (long arrows) in different “centers” of our FOV, and some contours are associated with some of those divergences, it is clear to observe that there are not strong magnetic elements associated to these emergences, which is only possible to observe in the region of interest where AR 11190 is starting the formation.

5. CONCLUSIONS

During the formation stage of solar active regions, it is possible to distinguish how the proper motions of the plasma (continuum images) within the region of interest are affected by the emergence of new magnetic field. However, it is not possible to say the same in the contrary sense, due to, even where it would be possible to observe strong divergences of plasma, there are not emergences of new and strong positive magnetic elements in such regions.

Generally, the flow fields comprise, in the case of active regions, stronger magnetic elements, which are often also of bipolar nature showing a way-more turbulent behavior than their corresponding counterparts in the quiet Sun. A more detailed study about the dynamics and the behavior of the connection between the plasma motions with the emergence of new magnetic fields is described in *Campos Rozo et al. 2018a*.

A similar study was performed in order to compare the behavior during the formation of an AR and the evolution of proper motions within a Quiet Sun region (*Campos Rozo et al. 2018b*)

Acknowledgments

We acknowledge the support of FWF project P27800. HMI/SDO data were obtained from the Joint Science Operation Center (JSOC), and they are courtesy of NASA/SDO and the AIA, EVE, and HMI science teams

REFERENCES

- [1] The SunPy Community, et al. Sunpy-Python for Solar Physics, APJ - Computational Science and Discovery, 8.
- [2] Palacios, J., Blanco Rodríguez, J., Vargas Domínguez, S., et al. 2012, A&A, 537, A21.
- [3] November, L. J. and Simon, G. W.: 1988, Astrophys. J. 333, 427.
- [4] November, L. J., Toomre, J., Gebbie, K. B., Simon, G. W. 1981, ApJ, 245, L123-L126.
- [4] Domínguez Cerdeña, I. 2003, A&A, 412, L65.
- [5] Title, A. M., Tarbell, T. D., Topka, K. P., Ferguson, S. H., Shine, R. A., and SOUP Team (1989). Statistical properties of solar granulation derived from the SOUP instrument on Spacelab 2. ApJ, 336:475-494.
- [6] Ishikawa, R. & Tsuneta, S. 2011, ApJ, 735, 74.
- [7] Utz, D., Hanslmeier, A., Muller, R., Veronig, A., Rybák, J., and Muthsam, H. 2010, A&A, 511, A39.
- [8] Solanki, S. K. 2003. Sunspots: An overview. A&A Reviews, 11, 153-286.
- [9] Diaz Bazo, C. J. & Asensio Ramos, A. 2018, A&A, 614, A5.
- [11] Hill, F., Gough, D., Toomre, J. 1984, Mem S. A. It., 55, 153-161.
- [12] Rast, M. P. 2003, ApJ, 597, 1200-1210.
- [13] Hoeksema J. T., Y. Liu, K. Hayashi et al. (2014). The Helioseismic and Magnetic Image (HMI) Vector Magnetic Field Pipeline: SHARPs – Space- Weather HMI Active Region Patches, Sol. Phys. 289, 3549.
- [14] Pesnell, W. D., B. J. Thompson, P.C. Chamberlin (2012). The Solar Dynamics Observatory (SDO), Sol. Phys. 275, 3.
- [15] Campos Rozo, J. I., D. Utz, S. Vargas-Domínguez, A. Veronig, T. Van Doorsselaere 2018, A&A Photospheric plasma and magnetic field dynamics during the formation of solar AR 11190, under review.
- [16] Campos Rozo, J. I., D. Utz, A. Veronig, S. Vargas-Domínguez, Proceedings Workshop “Solar Influence on the Magnetosphere, Ionosphere and Atmosphere”. Vol. 10, p. 37-42. ISSN 2367-7570